Journal of Power Sources 196 (2011) 7006–7010

Contents lists available at ScienceDirect

Journal of Power Sources

journal homepage: www.elsevier.com/locate/jpowsour

Short communication

Synthesis and electrochemical properties of a porous titania fabricated from exfoliated nanosheets

Norihito Kijima[a,*], Mitsuhiro Kuwabara[a,b], Junji Akimoto[a], Toshiya Kumagai[a,b], Kaoru Igarashi[b], Tadao Shimizu[b]

[a] National Institute of Advanced Industrial Science and Technology (AIST), Tsukuba Central 5, 1-1-1 Higashi, Tsukuba, Ibaraki 305-8565, Japan
[b] Chiba Institute of Technology, 2-17-1 Tsudanuma, Narashino, Chiba 275-0016, Japan

ARTICLE INFO

Article history:
Received 21 August 2010
Received in revised form 2 October 2010
Accepted 4 October 2010
Available online 13 October 2010

Keywords:
Nanosheets
Porous titanium
Lithium battery

ABSTRACT

In order to obtain a new type of lithium battery electrode material with high capacity, a porous titania was fabricated from exfoliated nanosheets. Nitrogen adsorption–desorption isotherms showed that the porous titania has a mesoporous structure composed of slit-shaped pores. The porous titania worked as a rechargeable electrode material. An initial capacity of 267 mAh g^{-1} (cut-off voltage: 1.0 V) could be achieved, which approximately correspond to the composition of $Li_{0.8}TiO_2$. A charge–discharge test between 3 V and 1 V gave a good rechargeable capacity of about 200 mAh g^{-1} over the first 10 cycles. The porous titania had a larger capacity than the parent unexfoliated $H_{1.08}Ti_{1.73}O_4$ specimen. There was no correlation between the mesopore volume and the capacity. The development of smaller fine pores below the mesopores contributed to obtaining the high capacity.

© 2010 Elsevier B.V. All rights reserved.

1. Introduction

Nanomaterials have the potential to deliver a step change in the performance of rechargeable lithium batteries [1]. These materials could enable the development of a new generation of rechargeable lithium batteries, which are essential for electric vehicles and clean energy storage. These batteries have significantly less impact on the environment and can thus help reduce global warming.

Nanostructured titanium oxide-based materials have been widely studied and are considered good alternatives to the carbon-based anode materials in some Li-ion batteries [2]. Titanium oxide-based anodes exhibit a relatively high voltage vs. Li (1–2 V), which helps to avoid a solid electrolyte interface (SEI) layer formation, making the battery much safer than the graphite anodes used commercially.

Titania nanosheets are a promising active material candidate for the lithium-ion secondary battery because a large amount of lithium can be stored in a nanospace constructed with nanosheets. Extensive studies of titania nanosheets have been reported by many researchers over the past several years. Although various physical properties of titania nanosheets have been investigated [3], these has been little reported research on the application of titania nanosheets and other oxide nanosheets as an active material for the lithium secondary battery [4–6].

We recently succeeded in synthesizing a large amount of thin flake titania by freeze-drying titania nanosheets exfoliated by $C_2H_5NH_3OH$. The freeze-dried titania nanosheets acted as a rechargeable active material in a liquid organic electrolyte lithium cell [4]. In order to improve the battery performance of the titania nanosheets, we attempted to control the nanospace constructed with nanosheets.

The exfoliated nanosheets can be precipitated by the addition of cations such as H^+. Application of this exfoliation-precipitation method would enable new types of nanomaterials to be created. Abe et al. attempted to construct a new porous material by exfoliation of the $K_4Nb_6O_{17}$ sheets and by precipitation with MgO fine particles [7]. We adapted this synthetic technique to obtain a new type of porous titania. The synthesis procedure to produce the porous titania fabricated from exfoliated nanosheets is summarized in Fig. 1.

In this article, we report the synthesis and electrochemical properties of the porous titania fabricated from exfoliated nanosheets. The porous titania had a larger capacity than the unexfoliated parent material. The porous titania worked as a rechargeable electrode material, and a good rechargeable capacity of about 200 mAh g^{-1} was obtained over the first 10 cycles.

2. Experimental

The starting layered material, $K_{0.81}Ti_{1.73}Li_{0.27}O_4$, was prepared by a conventional solid state reaction. A stoichiometric mixture of K_2CO_3, Li_2CO_3, and TiO_2 (anatase form) was calcined at

* Corresponding author.
E-mail address: n-kijima@aist.go.jp (N. Kijima).

0378-7753/$ – see front matter © 2010 Elsevier B.V. All rights reserved.
doi:10.1016/j.jpowsour.2010.10.022

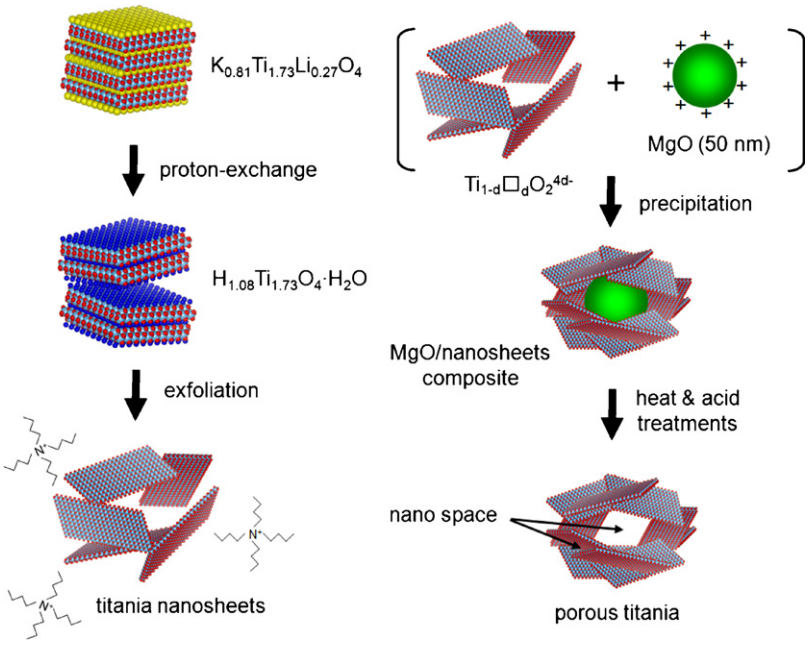

Fig. 1. Scheme of the synthetic process of a porous titania fabricated from exfoliated nanosheets.

1100 °C for 10 h. The material obtained was then converted into its proton-exchanged form, $H_{1.08}Ti_{1.73}O_4{\cdot}H_2O$ [8]. Twenty grams of the $K_{0.81}Ti_{1.73}Li_{0.27}O_4$ powder was stirred in 2000 cm^3 of 1 mol dm^{-3} HCl aqueous solution at room temperature for 1 d. After four times repetition of this acid treatment, the product was filtered and washed with a copious amount of distilled water to eliminate excess acid, and then air dried.

The exfoliation of the titania nanosheets was carried out in aqueous tetrabutylammonium hydroxide, $(C_4H_9)_4NOH$, solution. The $H_{1.08}Ti_{1.73}O_4{\cdot}H_2O$ powder was added to the aqueous solution, which contained 5 times more $(C_4H_9)_4NOH$ in molar quantity than the $H_{1.08}Ti_{1.73}O_4{\cdot}H_2O$ powder. The mixture was then agitated vigorously for 12 d at room temperature. To remove unexfoliated nanosheets, the suspension was centrifuged at 2000 rpm, and the precipitation was eliminated from the suspension.

A porous titania was fabricated from the exfoliated nanosheets. The same weight of MgO fine particles (ca. 50 nm, Ube Industry Ltd.) as $H_{1.08}Ti_{1.73}O_4{\cdot}H_2O$ was added to the suspension. The mixture was stirred for 2 h at room temperature, and then kept for several hours without agitation until precipitation formed. The composite of exfoliated nanosheets and MgO particles was then filtered and evacuated at various temperatures for 1 h. To obtain porous materials that consist of only titania sheets by removal of MgO particles, the specimens were stirred in 1 mol dm^{-3} HCl aqueous solution at room temperature for 1 d. After the acid treatment, the products were filtered and washed with distilled water, and then air dried.

X-ray powder diffraction (XRD) data were collected on a Bragg–Brentano-type powder diffractometer (Rigaku RINT-2550VHF) with Cu Kα radiation. Scanning electron microscopy (SEM) images were obtained using a JEOL JSM-5400 microscope equipped with an EDX analyzer (JED-2100). Scanning transmission electron microscopy (STEM) images were taken with a HITACHI S-6800 microscope. Nitrogen adsorption-desorption isotherms of the products were obtained on a BEL Japan BELSORP-mini II apparatus. Before the measurements, the powder specimens were outgassed at 300 °C for 60 min below 1 Pa. The surface area was calculated by the Brunauer–Emmett–Teller (BET) method [9], and the pore size distribution was obtained by the Dollimore and Heal (DH) method [10].

Charge–discharge measurements were performed in the galvanostatic mode using charge–discharge equipment (Nagano Co., Ltd., BTS-2004W) at 25 °C in a thermostatic chamber maintained within ±1.0 °C. The working electrode consisted of active material, acetylene black (DENKA BLACK), and polytetrafluoroethylene (PTFE) powders at a weight ratio of 6:3:1. The mixture was pressed onto Al grids under a pressure of 100 MPa. The electrode was then dried at 120 °C for 1 d under vacuum and moved to a glove box filled with Ar gas (−88 °C dew point) without exposure to air. The counter electrode was Li foil, and the separator was a microporous polypropylene sheet (SELGARD, #2400). The electrolyte was a 1 mol dm^{-3} solution of $LiPF_6$ in blended ethylene carbonate (EC) and diethyl carbonate (DEC) with a volumetric EC:DEC ratio of 1:1. The cells used for the measurements were constructed in a stainless steel test cell (HS flat test cell, Hohsen Corp.). The cells were fabricated in an argon-filled glove box.

3. Results and discussion

XRD data confirmed that single phase specimens of the starting material $K_{0.81}Ti_{1.73}Li_{0.27}O_4$ and its proton-exchanged form $H_{1.08}Ti_{1.73}O_4{\cdot}H_2O$ were synthesized. EDX analyses of the starting material and the proton-exchanged specimen confirmed that almost 100% of K^+ was exchanged. All diffraction peaks of both compounds were indexed on the orthorhombic symmetry [8]. Lattice constants were $a = 3.825$ Å, $b = 15.553$ Å, and $c = 2.970$ Å for $K_{0.81}Ti_{1.73}Li_{0.27}O_4$ and $a = 3.782$ Å, $b = 18.473$ Å, and $c = 2.995$ Å for $H_{1.08}Ti_{1.73}O_4{\cdot}H_2O$, respectively. The lattice constants a and c were almost independent after the acid treatment, but b increased significantly. This increment of b indicates that the K^+ ions in interlayer in the layer structure of $K_{0.81}Ti_{1.73}Li_{0.27}O_4$ are exchanged by H_3O^+ ions. The presence of H_3O^+ ions and the H_2O molecule in the structure of $H_{1.08}Ti_{1.73}O_4{\cdot}H_2O$ is reported in the literature, and the extent of increase is in good agreement with the reported value [8].

Fig. 2(a) and (b) shows the SEM images of $K_{0.81}Ti_{1.73}Li_{0.27}O_4$ and $H_{1.08}Ti_{1.73}O_4{\cdot}H_2O$, respectively. Most of the $K_{0.81}Ti_{1.73}Li_{0.27}O_4$ particles had plate-like shapes. The particle size of $K_{0.81}Ti_{1.73}Li_{0.27}O_4$ was larger than that of our previously used starting material, $Cs_{0.68}Ti_{1.83}O_4$ [4], and wider nanosheets could therefore be

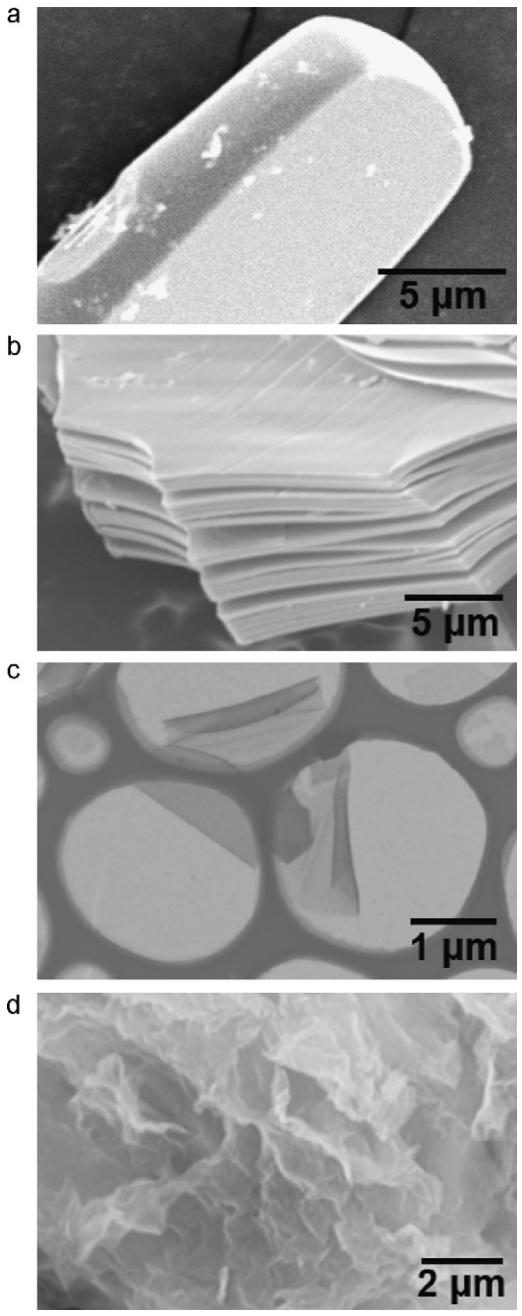

Fig. 2. SEM images of (a) $K_{0.81}Ti_{1.73}Li_{0.27}O_4$ and (b) $H_{1.08}Ti_{1.73}O_4{\cdot}H_2O$, (c) STEM image of titania nanosheets exfoliated by $(C_4H_9)_4NOH$ solution, and (d) SEM image of a porous titania fabricated from exfoliated nanosheets.

obtained. As Fig. 2(b) shows, the $H_{1.08}Ti_{1.73}O_4{\cdot}H_2O$ particles were partly exfoliated after the acid treatment. This finding shows that interlayer interactions weakened after the ion-exchange.

The STEM image of the titania nanosheets exfoliated by the $(C_4H_9)_4NOH$ solution is depicted in Fig. 2(c). The STEM image revealed that the titania nanosheets were partially self-rolled at the edges. Similar self-assembly was reported in the niobate sheets, which rolled into a loosely bound tubular structure [11].

In order to produce the porous titania, MgO fine particles (50 nm) were added to the colloidal suspension containing the titania nanosheets. Precipitation formed after the addition, and the supernatant liquid was transparent. The electrokinetic potential (ζ potential) of the MgO fine particles was reported to be +47.3 mV at pH 9.8 [5]. However, the titania nanosheets are known to have a

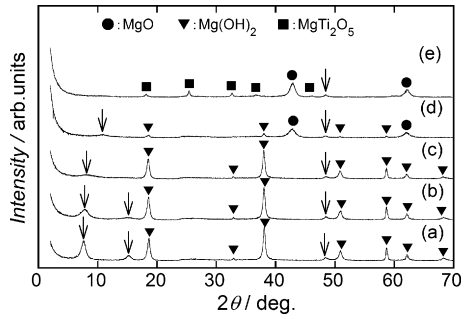

Fig. 3. XRD patterns of the MgO/nanosheet composite after evacuation at (a) room temperature, (b) 200 °C, (c) 300 °C, (d) 400 °C, and (e) 500 °C. The peaks indicated by arrows are those of the titania nanosheet.

negative charge in the $(C_4H_9)_4NOH$ solution [12]. Therefore, the MgO/nanosheet composite could be formed by the electrostatic force of attraction. In addition, no precipitation was formed when TiO_2 particles were used instead of MgO particles, because TiO_2 particles had negative ζ potentials at around pH 10.

Fig. 3 shows the XRD patterns of the MgO/nanosheet composite after evacuation at several temperatures. $Mn(OH)_2$ was detected at lower evacuation temperatures. The MgO additive changed to $Mg(OH)_2$ in the $(C_4H_9)_4NOH$ solution. After evacuation at 400 °C, this $Mg(OH)_2$ again changed to MgO, and reacted partially to form $MgTi_2O_5$ at 500 °C. The peaks that originated in the titania nanosheet are indicated by the arrows in Fig. 3. Their peak positions did not change below 300 °C. The colors of the samples after evacuations above 300 °C were dark gray, which is attributable to adhesion of the carbon deposit derived from the decomposition of $(C_4H_9)_4N^+$.

Fig. 4 presents the XRD patterns of the MgO/nanosheet composite after the acid treatments. As Fig. 4 shows, $Mg(OH)_2$ and MgO could be removed from the composites evacuated below 400 °C. Disappearance of the Mg element in these specimens was also confirmed by the EDX analyses. However, $MgTi_2O_5$ still remained in the composite evacuated at 500 °C before acid treatment. The peaks around $2\theta = 10°$ in Fig. 4 are associated with porous structures, which obviously shifted depending on the evacuation temperatures.

Table 1 lists the BET surface area and pore volume of the MgO/nanosheet composite before and after the acid treatments. Even after the acid treatments, the surface areas of the samples were still large. This finding shows that the large surface areas of the composites are associated not only with the surface area of the MgO particles, but also with that of the exfoliated nanosheets. After the acid treatments, the surface areas of the samples evacuated at room temperature increased significantly, but those of the other samples evacuated above 200 °C decreased. The increase or

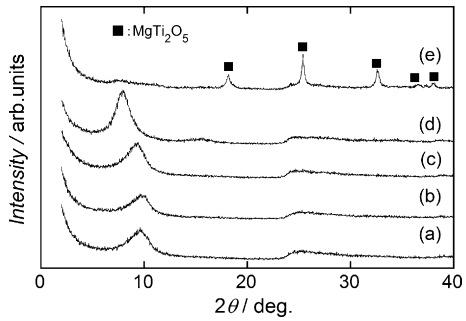

Fig. 4. XRD patterns of the MgO/nanosheet composite after acid treatments. Before acid treatments, the composites were evacuated at (a) room temperature, (b) 200 °C, (c) 300 °C, (d) 400 °C, and (e) 500 °C.

Table 1
BET surface area (S_{BET}) and pore volume (V_P) of the MgO/nanosheet composite before and after the acid treatments.

Evacuation temperature (°C)	Before acid treatment		After acid treatment	
	S_{BET} ($m^2\ g^{-1}$)	V_P ($cm^3\ g^{-1}$)	S_{BET} ($m^2\ g^{-1}$)	V_P ($cm^3\ g^{-1}$)
Room temp.	88	0.63	105	0.36
200	112	0.71	99	0.43
300	122	0.45	96	0.52
400	172	0.54	84	0.52
500	138	0.57	108	0.67

decrease of the surface areas is attributable to the destruction of the titania nanosheets, desorption and decomposition of $(C_4H_9)_4N^+$, and/or elution of MgO and $Mg(OH)_2$.

The pore volumes of the samples after the acid treatments gradually increased as the evacuation temperature increased. This increment of pore volumes is associated with the elution of MgO or $Mg(OH)_2$ from the composites. On the other hand, no correlation between the evacuation temperatures and the pore volumes was identified in the samples before the acid treatments.

Fig. 5 shows the nitrogen adsorption–desorption isotherms and pore size distributions of the porous titania and the parent unexfoliated $H_{1.08}Ti_{1.73}O_4{\cdot}H_2O$ specimen. This porous titania specimen was prepared by acid treatment after evacuation at room temperature. The surface area and pore volume of the porous titania are listed in Table 1. Those values increased significantly in comparison with the parent $H_{1.08}Ti_{1.73}O_4{\cdot}H_2O$ specimen. The BET surface area of $H_{1.08}Ti_{1.73}O_4{\cdot}H_2O$ was 8 $m^2\ g^{-1}$, and its pore volume was 0.05 $cm^3\ g^{-1}$.

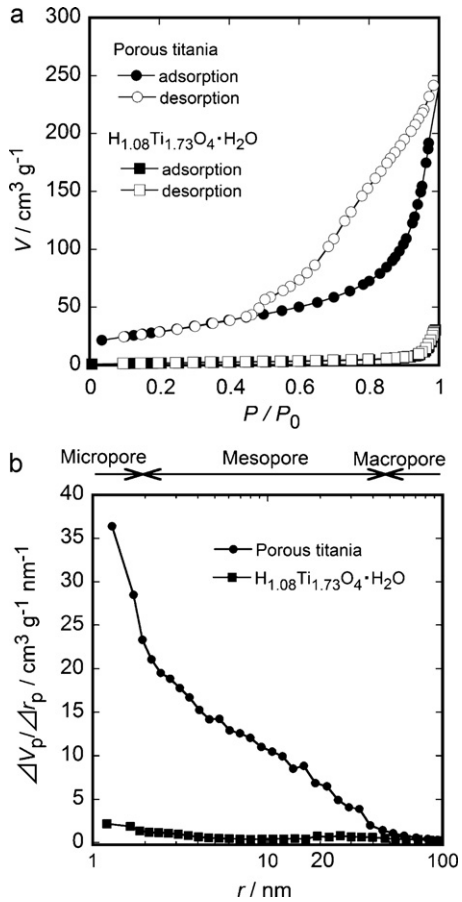

Fig. 5. Nitrogen adsorption–desorption isotherms and pore size distributions of (a) the porous titania and (b) the parent unexfoliated $H_{1.08}Ti_{1.73}O_4{\cdot}H_2O$ specimen.

The nitrogen adsorption–desorption isotherms of the porous titania had a large hysteresis loop, which indicates the presence of mesopores. According to the IUPAC classification [9], the hysteresis loop was classified as typical type H3. The type H3 hysteresis loop is associated with the presence of slit-shaped pores [9].

As shown in Fig. 5(b), the porous titania was composed of both micropores and mesopores. No distribution peak corresponding to the space preserved by MgO particles (50 nm) existing between the titania nanosheets was obtained. In this work, the pore size distribution of the samples could not be controlled because MgO changed to $Mg(OH)_2$ in the $(C_4H_9)_4NOH$ solution.

Fig. 6(a) gives the charge–discharge curves of the porous titania over the first 10 cycles. This porous titania was prepared by acid treatment after evacuation at room temperature, and SEM image and XRD data of the porous titania are shown in Fig. 2(d) and Fig. 4(a), respectively. The porous titania worked as a rechargeable electrode material, as Fig. 6(a) shows. An initial capacity of 267 mAh g^{-1} (cut-off voltage: 1.0 V) could be achieved, which approximately correspond to the composition of $Li_{0.8}TiO_2$. The capacity on the second cycle was 214 mAh g^{-1}, and thereafter

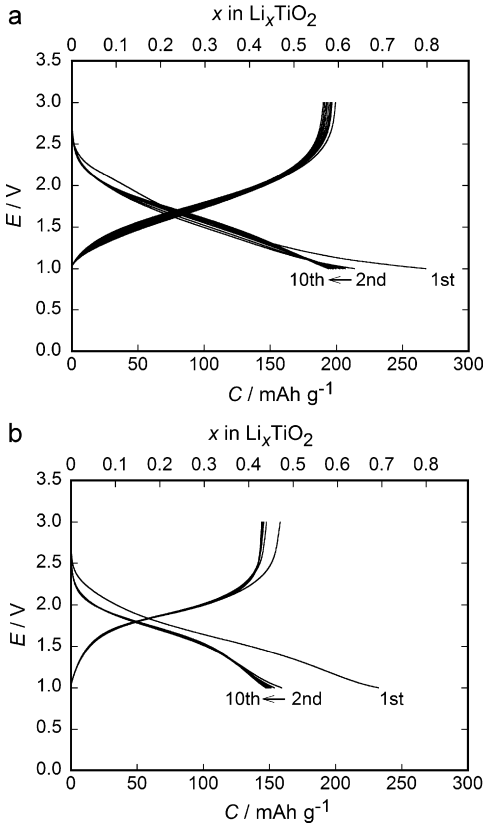

Fig. 6. Charge–discharge curves of (a) the porous titania and (b) the parent unexfoliated $H_{1.08}Ti_{1.73}O_4{\cdot}H_2O$ specimen over the first 10 cycles; voltage, 1.0–3.0 V; current rate, 10 mAh g^{-1}.

the cell stabilized, yielding an almost constant capacity of about 200 mAh g^{-1} for 10 cycles. The rechargeable capacity of the porous titania was higher than that of the freeze-dried product of the titania nanosheets [4]. The charge–discharge profiles of the porous titania showed gently sloping curves, although most titanium oxides, such as TiO_2 (anatase) and $Li_4Ti_5O_{12}$ (spinel), have plateau voltages.

Fig. 6(b) presents the charge–discharge curves of the parent unexfoliated $H_{1.08}Ti_{1.73}O_4{\cdot}H_2O$ specimen over the first 10 cycles. Charge–discharge tests between 3 V and 1 V gave a relatively high capacity of about 150 mAh g^{-1} over the first 10 cycles, although the surface area and pore volume of the parent specimen were much smaller than those of the porous titania. The shape of the charge–discharge curve of the porous titania approached that of the parent $H_{1.08}Ti_{1.73}O_4{\cdot}H_2O$ specimen during the charge–discharge cycling. This observation suggests that the ordering of loosely-structured nanosheets was caused by lithium insertion, because the exfoliated nanosheets can be precipitated by Li^+ ions.

The other MgO/nanosheet composites after acid treatment also worked as electrode materials. Nonetheless the pore volumes of these samples increased, and their rechargeable capacities decreased with a rise of the evacuation temperatures. This finding shows that there is no correlation between the porosity and the capacity. The development of smaller ultrafine pores below mesopores would contribute to obtaining a high capacity. Thus, to enhance the electrochemical performance of the porous titania electrode, one task for future research would be to modify and optimize the ultrafine pores.

Acknowledgements

A part of this work was conducted at the Nano-Processing Facility, supported by IBEC Innovation Platform, AIST.

References

[1] P.G. Bruce, B. Scrosati, J.-M. Tarascon, Angew Chem. Int. Ed. 47 (2008) 2930.
[2] Z. Yang, D. Choi, S. Kerisit, K.M. Rosso, D. Wang, J. Zhang, G. Graff, J. Liu, J. Power Sources 192 (2009) 588.
[3] M. Osada, T. Sasaki, J. Mater. Chem. 19 (2009) 2503.
[4] N. Kijima, Y. Takahashi, H. Hayakawa, J. Awaka, J. Akimoto, J. Phys. Chem. Solids 69 (2008) 1447.
[5] L. Wang, K. Takada, A. Kajiyama, M. Onoda, Y. Michiue, L. Zhang, M. Watanabe, T. Sasaki, Chem. Mater. 15 (2003) 4508.
[6] S. Suzuki, M. Miyayama, J. Phys. Chem. B 110 (2006) 4731.
[7] R. Abe, K. Shinohara, A. Tanaka, M. Hara, J.N. Kondo, K. Domen, Chem. Mater. 9 (1997) 2179.
[8] T. Sasaki, F. Kooli, M. Iida, Y. Michiue, S. Takenouchi, Y. Yajima, F. Izumi, B.C. Chakoumakos, M. Watanabe, Chem. Mater. 10 (1998) 4123.
[9] K.S.W. Sing, D.H. Everett, R.A.W. Haul, L. Moscou, R.A. Pierotti, J. Rouquėrol, T. Siemieniewska, Pure Appl. Chem. 57 (1985) 603.
[10] (a) D. Dollimore, G.R. Heal, J. Appl. Chem. 14 (1964) 109;
(b) D. Dollimore, G.R. Heal, J. Colloid Interface Sci. 33 (1970) 508.
[11] G.B. Saupe, C.C. Waraksa, H.-N. Kim, Y.J. Han, D.M. Kaschak, D.M. Skinner, T.E. Mallouk, Chem. Mater. 12 (2000) 1556.
[12] T. Sasaki, M. Watanabe, J. Phys. Chem. B 101 (1997) 10159.